



## Comparison of Structural Changes in Fully Delithiated $\text{Li}_x[\text{Ni}_{1/3}\text{Co}_{1/3}\text{Mn}_{1/3}]\text{O}_2$ and $\text{Li}_x[\text{Ni}_{0.33}\text{Co}_{0.33}\text{Mn}_{0.30}\text{Mg}_{0.04}]\text{O}_{1.96}\text{F}_{0.04}$ Cathodes ( $x = 0$ ) upon Thermal Annealing

Yoojung Kim,<sup>a</sup> Junho Eom,<sup>a</sup> Min Gyu Kim,<sup>b</sup> Yang-Kook Sun,<sup>c,\*</sup>  
Chong Seung Yoon,<sup>d</sup> and Jaephil Cho<sup>\*,z</sup>

<sup>a</sup>Department of Applied Chemistry, Kumoh National Institute of Technology, Gumi, Korea

<sup>b</sup>Beamline Research Division, Pohang Accelerator Laboratory, Pohang University of Science and Technology, Pohang, Korea

<sup>c</sup>Department of Chemical Engineering, and <sup>d</sup>Division of Materials Science and Engineering, Hanyang University, Seoul, Korea

This study compared the structural changes in  $\text{Li}_x[\text{Ni}_{1/3}\text{Co}_{1/3}\text{Mn}_{1/3}]\text{O}_2$  and  $\text{Li}_x[\text{Ni}_{0.33}\text{Co}_{0.33}\text{Mn}_{0.30}\text{Mg}_{0.04}]\text{O}_{1.96}\text{F}_{0.04}$  cathodes ( $x = 0$ ) occurring after full delithiation and subsequent heat-treatment at 200, 300, and 400°C using X-ray diffraction (XRD), transmission electron microscopy, and X-ray absorption spectra (XAS). In both cathodes, XRD patterns at  $x = 0$  showed a layered O3-type structure ( $\text{CdCl}_2$ ), but subsequent thermal annealing led to a similar structure decomposition to a  $\text{Co}_3\text{O}_4$ -type spinel and possible new O3- $\text{Ni}_{1/3}\text{Mn}_{1/3}\text{O}_{2+8}$ -type layered phases. However, the XAS spectra clearly showed that the  $\text{Li}_x[\text{Ni}_{0.33}\text{Co}_{0.33}\text{Mn}_{0.30}\text{Mg}_{0.04}]\text{O}_{1.96}\text{F}_{0.04}$  exhibited much improved structural stability, showing a suppression of the phase decomposition to spinel  $\text{Co}_3\text{O}_4$ , as evidenced by a decrease in the FT peak intensity of corner-shared  $\text{CoO}_6$  octahedra at  $\sim 3.2 \text{ \AA}$ . © 2007 The Electrochemical Society. [DOI: 10.1149/1.2724761] All rights reserved.

Manuscript submitted October 2, 2006; revised manuscript received February 8, 2007. Available electronically April 19, 2007.

The greatest concern with  $\text{LiCoO}_2$  cathodes is the rapid capacity fading that occurs at higher voltages due to Co dissolution associated with structure distortion and thermal runaway under thermal abuse at the overcharged states, such as 12 V overcharge and nail penetration.<sup>1-6</sup> The triggering mechanism that induces thermal runaway is directly related to the extent of cathode thermal instability at the charged states, and more lithium deintercalation results in increased oxygen generation from the cathodes. However, most studies which aim at overcoming the inherent cathode problems focus on retarding the flammable nature of the electrolyte.<sup>7</sup> On the other hand, a surface coating is an alternative solution, not only for enhancing the cycle life at 4.6 and 4.8 V, but also for removing the thermal instability of the cathodes resulting from oxygen evolving from the cathodes.<sup>8-15</sup>

Maleki et al. reported that the lower oxygen generation in the  $\text{AlPO}_4$ -coated  $\text{Li}_x\text{CoO}_2$  rather than the bare  $\text{Li}_x\text{CoO}_2$  both at 4.3 and 4.6 V was due to the predominant presence of the  $\text{Co}_3\text{O}_4$  phase compared with the spinel  $\text{Li}_x\text{Co}_2\text{O}_4$  phase.<sup>16</sup> However, Lee et al. reported that the better thermal stability of the  $\text{Li}_x\text{Ni}_{0.85}\text{Co}_{0.15}\text{O}_2$  cathode over the  $\text{Li}_x\text{NiO}_2$  cathode originated from the formation of  $\text{Co}_3\text{O}_4$  rather than the NiO-type rock salt phase below 4.6 V.<sup>17</sup> Cho et al. compared the heat generation of  $\text{Li}_x\text{Ni}_{0.8}\text{Co}_{0.1}\text{Mn}_{0.1}\text{O}_2$  and  $\text{Li}_x\text{CoO}_2$  as a function of  $x$ . As opposed to  $\text{Li}_x\text{CoO}_2$  with decreasing  $x$ , this shows continuous oxygen evolution as the temperature increases from 200°C to 350°C.<sup>4,5</sup> The first phase showed maximum heat generation at  $x \sim 0.4$ , and after which the heat generation decreases as  $x$  approaches 0.2. This result is consistent with a 12 V thermal abuse test that did not show thermal runaway of the cell containing  $\text{Li}_x\text{Ni}_{0.8}\text{Co}_{0.1}\text{Mn}_{0.1}\text{O}_2$ .

Recently, it was reported that  $\text{Li}_x[\text{Ni}_{1/3}\text{Co}_{1/3}\text{Mn}_{1/3-x}\text{Mg}_x]\text{O}_{2-z}\text{F}_z$  cathodes are good candidates for overcoming such problems.<sup>18,19</sup> Belharouak et al. reported a structural transition of the  $\text{Li}_{0.55}\text{Ni}_{1/3}\text{Co}_{1/3}\text{Mn}_{1/3}\text{O}_2$  cathodes with and without electrolytes above 300°C.<sup>20</sup> The annealed delithiated cathode without the reacted electrolyte at 360°C retained the original hexagonal layered structure with an  $R\bar{3}m$  space group. However, the sample that reacted with the electrolyte at 400°C showed a drastic decomposition of the

$\text{Li}_{0.55}\text{Ni}_{1/3}\text{Co}_{1/3}\text{Mn}_{1/3}\text{O}_2$  to  $\text{MnCO}_3$  and NiO. Yet, the X-ray diffraction (XRD) analysis did not show any evidence for the formation of  $\text{Co}_3\text{O}_4$  as a result of the decomposition. In addition, the onset temperature of oxygen generation for the  $\text{Li}_{0.55}\text{Ni}_{1/3}\text{Co}_{1/3}\text{Mn}_{1/3}\text{O}_2$  was  $\sim 280^\circ\text{C}$  while it was  $\sim 200^\circ\text{C}$  for  $\text{LiNi}_{0.85}\text{Co}_{0.1}\text{Al}_{0.05}\text{O}_2$ , demonstrating the higher thermal stability of the material and implying no possible explosion during nail penetration. In addition, a result similar to that of Belharouak et al. was reported by Sun et al. in which there was an increased onset temperature with the addition Mg and F in the  $\text{Li}_{0.55}\text{Ni}_{1/3}\text{Co}_{1/3}\text{Mn}_{1/3}\text{O}_2$ . However, these studies did not report the structural changes of the materials at the fully delithiated state.

This study reports the structural changes in the  $\text{Li}_x[\text{Ni}_{1/3}\text{Co}_{1/3}\text{Mn}_{1/3}]\text{O}_2$  and  $\text{Li}_x[\text{Ni}_{0.33}\text{Co}_{0.33}\text{Mn}_{0.30}\text{Mg}_{0.04}]\text{O}_{1.96}\text{F}_{0.04}$  cathodes after full delithiation, followed by different heat-treatment temperatures up to 400°C.

### Experimental

$\text{Li}_x[\text{Ni}_{1/3}\text{Co}_{1/3}\text{Mn}_{1/3-x}\text{Mg}_x]\text{O}_{2-z}\text{F}_z$  powders were prepared from a stoichiometric mixture of co-precipitated  $[\text{Ni}_{1/3}\text{Co}_{1/3}\text{Mn}_{1/3-x}\text{Mg}_x](\text{OH})_2$  and LiOH, LiF at 1000°C for 10 h. A more detailed experimental procedure may be found in Ref. 16.

Cathodes for battery test cells were made from the active material ( $\sim 25 \text{ mg}$ ), super P carbon black (MMM, Belgium), and a polyvinylidene fluoride (PVdF) binder (Kureha Company) at a weight ratio of 96:2:2. A cathode-slurry was prepared by thoroughly mixing an *N*-methyl-2-pyrrolidone (NMP) solution with the PVdF, the carbon black and the powdery cathode-active material. The electrodes were prepared by coating the cathode-slurry onto an Al foil, followed by drying at 130°C for 20 min. Coin-type battery-test cells (size 2016) containing a cathode, a Li metal anode, and a microporous polyethylene separator were prepared in a helium-filled glove box. The electrolyte used was 1 M  $\text{LiPF}_6$  with ethylene carbonate/diethylene carbonate/ethylmethyl carbonate (EC/DEC/EMC) (30:30:40 vol %) (Cheil Industries, Korea). After addition of the electrolyte, the test cells were aged at room temperature for 24 h before commencing the electrochemical tests.

Li-ion cells with 20 mAh [ $3 \times 4 \text{ cm}$ ] were used for 5 V charging, and  $\text{Li}_{1.02}[\text{Ni}_{1/3}\text{Co}_{1/3}\text{Mn}_{1/3}]\text{O}_2$  and  $\text{Li}_{1.02}[\text{Ni}_{0.33}\text{Co}_{0.33}\text{Mn}_{0.30}\text{Mg}_{0.04}]\text{O}_{1.96}\text{F}_{0.04}$  were used as the cathode while the anode material was synthetic graphite. The fresh cells

\* Electrochemical Society Active Member.

<sup>z</sup> E-mail: jpcho@kumoh.ac.kr

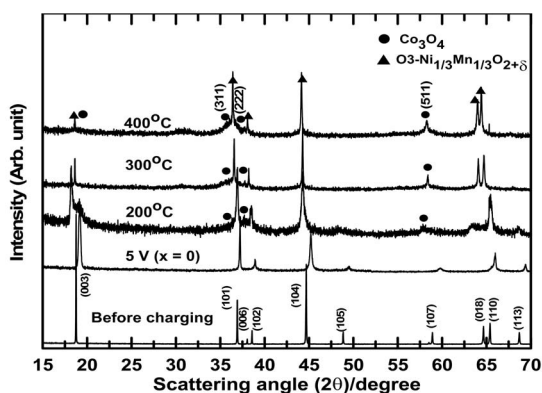


**Figure 1.** XRD patterns of the  $\text{Li}_x[\text{Ni}_{1/3}\text{Co}_{1/3}\text{Mn}_{1/3}\text{O}_2]$  cathodes before charging and after charging to 5 V, followed by respective heat-treatments at 200, 300, and 400°C.

were charged to 5 V at a rate of 0.05 C. At this voltage, the cell was maintained for 2 h under constant voltage mode, and the cell was disassembled and took the cathode from the cell. A typical weight of the composite was 40 mg and sealed in the pressure resistant Al pan in the glove box. The pan was heated at a rate of 5°C/min until the temperatures of 200, 300, or 400°C were reached. This temperature was then maintained for 30 min and then cooled to room temperature. The pan was disassembled, at which time the composite cathode was washed with DMC in the glove box and dried overnight at room temperature in the glove box.

Ex situ XRD measurements were performed using the composite electrode separated from the cell at designated cell potential. XRD patterns were obtained using  $\text{Cu K}\alpha$  X-source on Rigaku instrument operated at 11 kW. High-resolution transmission electron microscopy (HRTEM) samples were prepared by the evaporation of the dispersed composite cathodes in acetone on carbon-coated copper grids. The field-emission electron microscope was a JEOL 2000F operating at 200 kV. Inductively coupled plasma-mass spectroscopy (ICP, ICPS-1000IV, Shimadzu) was used to determine the Li content. The results of an ICP-MS analysis of the cathodes showed no trace of Li in the cathodes after a 5 V charge. The Co/Ni/Mn K-edge X-ray absorption spectroscopic (XAS) study for the thermal phase transition of the samples were carried out on the BL7C (Electrochemistry) beamline at the Pohang Light Source (PLS), which is a third generation synchrotron radiation source, in the 2.5 GeV storage ring with a ring current of 120–170 mA. A Si(111) double crystal monochromator was used to monochromatize the X-ray photon energy. Higher ordered harmonic contaminations were eliminated by detuning the monochromator to reduce the incident X-ray intensity by ~30%. The incident X-ray intensity was monitored using pure nitrogen gas-filled ionization chambers. The spectroscopic data were collected in transmittance mode. The energy calibration was made using standard Co, Mn, and Ni metal foils.

### Results and Discussion

Figure 1 shows the XRD patterns of the  $\text{Li}_x\text{Ni}_{1/3}\text{Co}_{1/3}\text{Mn}_{1/3}\text{O}_2$  cathodes after charging to 5 V, where  $x = 0$ , with a subsequent heat-treatment at 200, 300, and 400°C. The as-prepared cathode showed a high crystallinity with sharp peaks whose positions matched those of  $\text{LiCoO}_2$ , which has a space group of  $R\bar{3}m$ . After charging to 5 V, the peaks' broadening and obvious shifts to the right indicated a contraction of the lattice constants and the development of structural defects, respectively. In addition, the merging of split peaks in the (006)/(102) and (018)/(110) indicates possible cation-mixing. The Rietveld refinement was performed to identify the structural modification after a 5 V charge, and the  $a$  and  $c$  values of the samples before and after the 5 V charge were 2.858 and 14.223 Å and 2.832 and 13.938 Å, respectively. The decrease in the lattice volume was

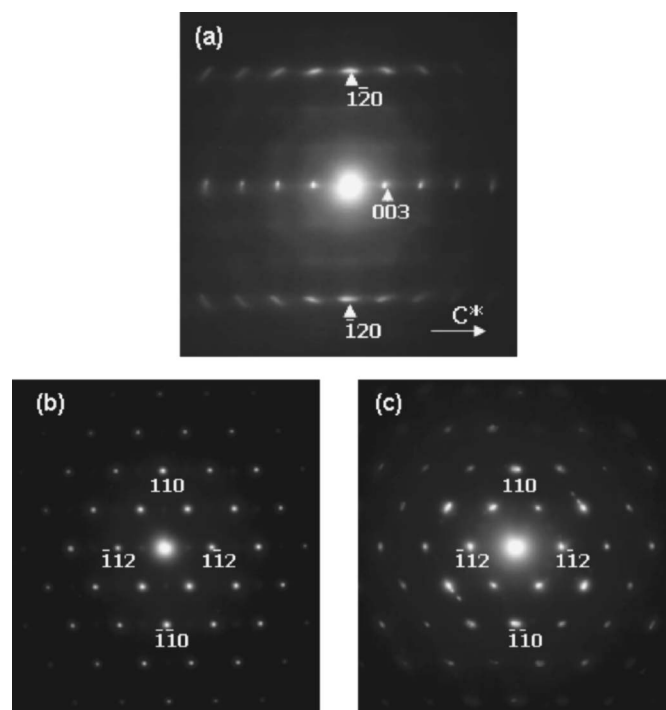
**Table I.** Rietveld refinement results of  $\text{Li}_x\text{Ni}_{1/3}\text{Co}_{1/3}\text{Mn}_{1/3}\text{O}_2$  at 5 V charging.

	$a$ (Å)	$c$ (Å)	Volume (Å <sup>3</sup> )	M in Li layer	$R_p$ (%) $R_{wp}$
Before charging	2.858(2)	14.223(2)	100.612(3)	0.008	13.1
					11.5
					3.9
5 V	2.832(4)	13.938(2)	96.835(3)	0.120	14.9
					12.5
					4.6

concomitant with a significantly increased metal fraction in the Li sites, showing a large degree of cation-mixing, as shown in Table I. Amatucci et al. report that fully delithiated  $\text{NiO}_2$  remains as a three layered O3-type structure ( $\text{CdCl}_2$ ) and does not convert to a single-layered O1-type ( $\text{CdI}_2$ ) structure as it did in  $\text{LiCoO}_2$ .<sup>21</sup> The presence of significant amounts of octahedrally coordinated metals in the empty lithium layer ( $3a$ ) might stabilize the O3-type structure. This inference is reinforced by the refinement results and that before charging, the amount of metals in the Li sites was 0.01 but rapidly increased to 0.12 after charging to 5 V.

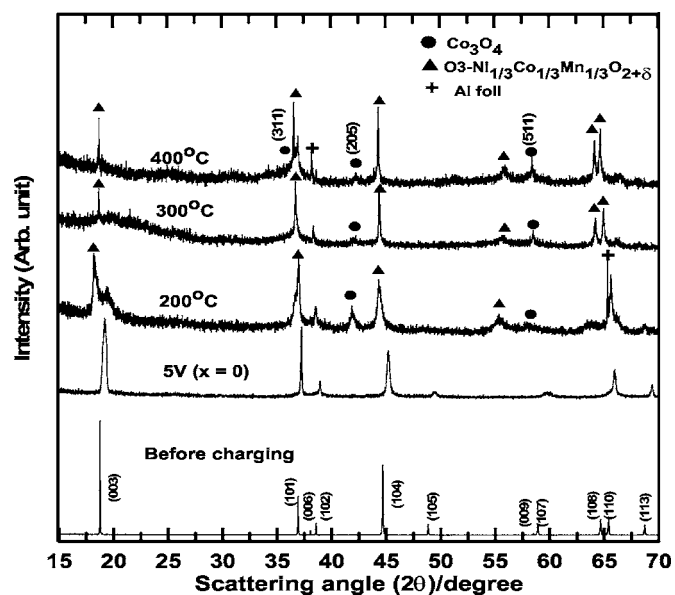
Peak-broadening is associated with structural defects, and the structural defects after charging were investigated by fitting five peaks ((0 0 3), (1 0 1), (1 0 4), (0 1 5) and (0 1 8)) using the XRD patterns. The peak widths  $\Delta k$  (full width at half-maximum) were fitted for each peak with a scattering vector  $k = (4\pi/\lambda)\sin\theta$  using a double-peak Lorentzian function for  $K_{\alpha 1}$  and  $K_{\alpha 2}$ . The estimated averaged  $\Delta k$  values for before charging, and after charging to 5 V were 0.08 and 0.31, respectively, indicating that structural defects had developed. The inhomogeneity of the cationic distribution in specific planes in a structure also induced slight modifications of the atomic positions that led to a distribution of  $d$ -spacing distances causing broadening of some specific diffraction peaks. The cathode that was heat-treated at 200°C showed a much lower peak intensity of the (003) peak, which was accompanied by a simultaneous increase in the intensity of a new peak at 18.2°. In addition, a  $\text{Co}_3\text{O}_4$ -like spinel phase ( $Fd\bar{3}m$ ) was formed which may be a result of a partial decomposition of the  $\text{Ni}_{1/3}\text{Co}_{1/3}\text{Mn}_{1/3}\text{O}_2$ . More structural details were investigated using TEM, and Fig. 2a shows an electron diffraction pattern (EDP) from a single  $\text{Li}_x\text{Ni}_{1/3}\text{Co}_{1/3}\text{Mn}_{1/3}\text{O}_2$  particle that had been charged to 5 V and heat-treated at 200°C along the [210] zone, showing that the  $R\bar{3}m$  symmetry was maintained in the particle. The streaks along the  $c$ -direction indicate the presence of stacking faults along the  $c$ -direction. In addition, the broadening of the (1–20) and (-120) spots suggest a relatively large spread in the lattice constant,  $a$ , resulting from cation-mixing within each layer. It appears that although the original  $R\bar{3}m$  symmetry was retained in this particle, the structure was highly disordered. Figures 2b and c show electron diffraction patterns obtained from two different  $\text{Li}_x\text{Ni}_{1/3}\text{Co}_{1/3}\text{Mn}_{1/3}\text{O}_2$  particles that had been charged to 5 V and heat-treated at 300°C in the [1–11] zone. While the particle in Fig. 2b retained a layered structure, some of the diffraction spots from the particle shown in Fig. 2c were split, unlike in Fig. 2b, suggesting the coexistence of two different structures in the particle represented in Fig. 2c. Indeed, the split peaks closely matched the spinel structure. Hence, the particle in Fig. 2c was partially transformed to the spinel structure. With increasing annealing temperature, the XRD diffraction patterns shows more developed a spinel  $\text{Co}_3\text{O}_4$  phase.

Figure 3 shows Ni, Co, Mn K-edge X-ray absorption near edge spectroscopy (XANES) spectra before charging, after charging to 5 V, and after annealing at 200, 300, and 400°C. The weak absorption peaks, A, represent the transition of a 1s electron to an unoccu-



**Figure 2.** Electron diffraction patterns of the  $\text{Li}_x\text{Ni}_{1/3}\text{Co}_{1/3}\text{Mn}_{1/3}\text{O}_2$  cathodes (a) after charging to 5 V with a subsequent heat-treatment at 200°C along the [210] zone. (b–c) Two different  $\text{Li}_x\text{Ni}_{1/3}\text{Co}_{1/3}\text{Mn}_{1/3}\text{O}_2$  particles that had been charged to 5 V and heat-treated at 300°C in the [1–11] zone.

piated molecular 3d orbital of the  $t_{2g}^3e_g^0$  electronic configuration for the  $\text{Mn}^{4+}$  ion,  $t_{2g}^6e_g^0$  for  $\text{Co}^{3+}$  ion, and  $t_{2g}^6e_g^2$  for  $\text{Ni}^{2+}$  ion, respectively. The shoulder peak, B, is related to a ligand to metal charge transfer process, and the peak, C, a 1s to 4p transition. Upon charging to 5 V in Co K-edge XANES spectra, the peaks shift to higher energies, but increasing the annealing temperature leads to a decrease in peaks



**Figure 4.** XRD patterns of the  $\text{Li}_x[\text{Ni}_{0.33}\text{Co}_{0.33}\text{Mn}_{0.3}\text{Mg}_{0.04}]\text{O}_{1.96}\text{F}_{0.04}$  cathodes ( $x = 0$ ) before charging and after charging to 5 V with subsequent heat-treatments at 200, 300, and 400°C.

position in A and B, approaching that of  $\text{Co}_3\text{O}_4$ . On the other hand, the Mn and Ni spectra after thermal annealing resembled that of the sample after a 5 V charge and before charging, respectively, indicating that the oxidation states of these were  $\text{Mn}^{4+}$  and  $\text{Ni}^{2+}$ , respectively. This meant that the Co ions were predominantly formed as the  $\text{Co}_3\text{O}_4$  phase while the Mn and Ni ions resided in the layered phase that may have the O3-type  $\text{Ni}_{1/3}\text{Mn}_{1/3}\text{O}_{2+\delta}$  phase.

Figure 4 exhibits XRD patterns of the  $\text{Li}_x[\text{Ni}_{0.33}\text{Co}_{0.33}\text{Mn}_{0.30}\text{Mg}_{0.04}]\text{O}_{1.96}\text{F}_{0.04}$ , where  $x = 0$  at different thermal annealing temperatures, and the overall peaks evolution was similar to that of  $\text{Li}_x[\text{Ni}_{1/3}\text{Co}_{1/3}\text{Mn}_{1/3}]\text{O}_2$ , showing the formation of

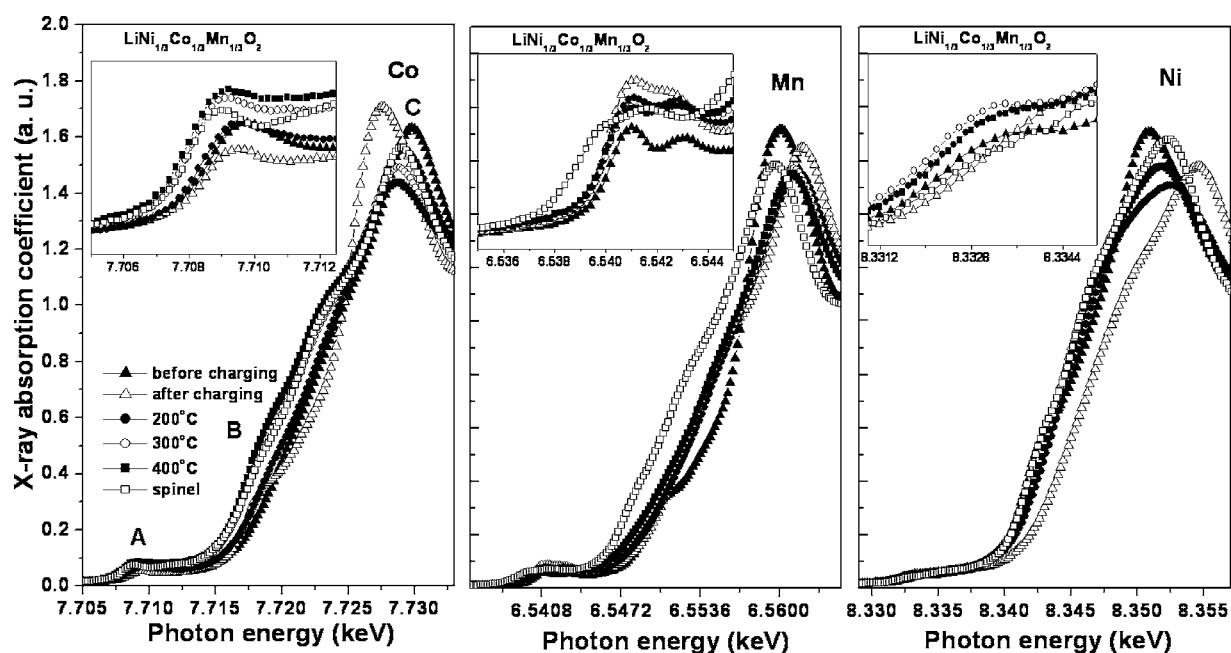


**Figure 3.** Ni, Co, Mn K-edge XANES spectra before charging, after charging to 5 V, after annealing at 200, 300, and 400°C in  $\text{Li}_x\text{Ni}_{1/3}\text{Co}_{1/3}\text{Mn}_{1/3}\text{O}_2$  cathodes ( $x = 0$ ).

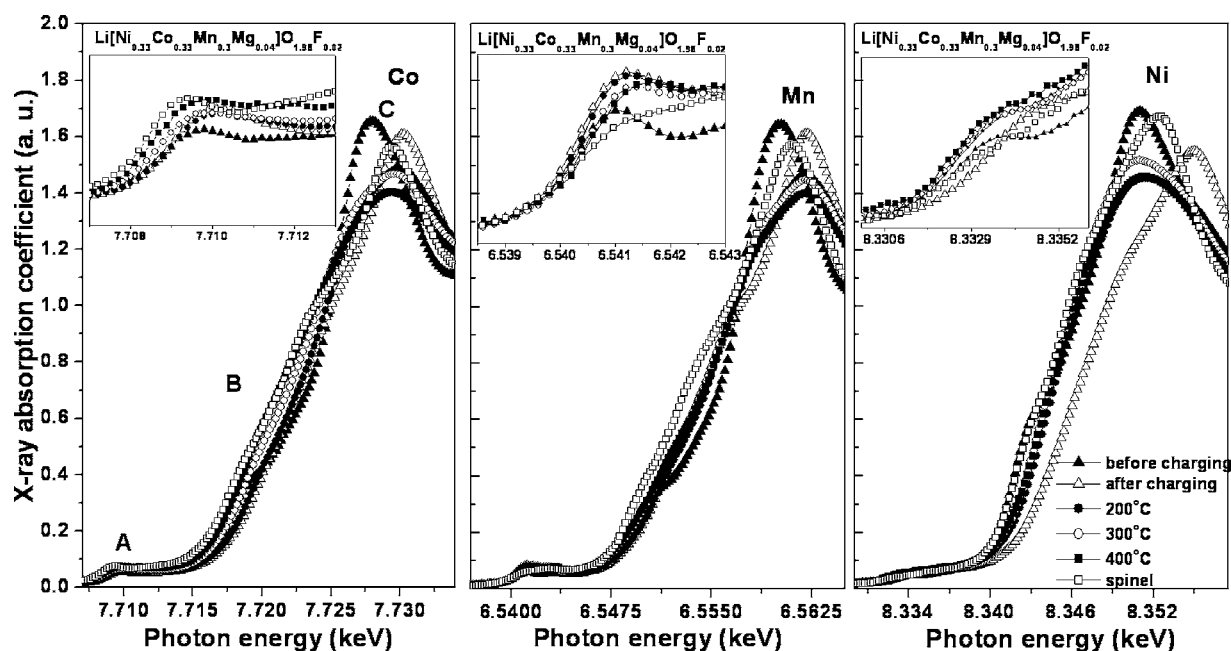


**Figure 5.** Ni, Co, Mn K-edge XANES spectra before charging, after charging to 5 V, after annealing at 200, 300, and 400°C in  $\text{Li}_x[\text{Ni}_{0.33}\text{Co}_{0.33}\text{Mn}_{0.3}\text{Mg}_{0.04}\text{O}]_{1.96}\text{F}_{0.04}$  cathodes.

both the  $\text{Co}_3\text{O}_4$  spinel and layered  $\text{O}3\text{-Ni}_{1/3}\text{Mn}_{1/3}\text{O}_{2+\delta}$  phase. Note, however, that there is a more developed, possible new  $\text{O}3\text{-Ni}_{1/3}\text{Mn}_{1/3}\text{O}_{2+\delta}$  phase in  $\text{Li}_x[\text{Ni}_{0.33}\text{Co}_{0.33}\text{Mn}_{0.30}\text{Mg}_{0.04}\text{O}]_{1.96}\text{F}_{0.04}$  than in  $\text{Li}_x[\text{Ni}_{1/3}\text{Co}_{1/3}\text{Mn}_{1/3}\text{O}]_2$ , as evidenced by the higher intensity peaks assigned to the layered phase at  $\sim 18.2^\circ$  and  $\sim 37^\circ$ . This demonstrated that Mg and F doping enhanced the structural integrity at higher temperatures, thus reducing decomposition to the  $\text{Co}_3\text{O}_4$ -type spinel phase. These results suggest that the layered phase observed in the XRD patterns of the doped cathode above 200°C may be  $\text{O}3\text{-Co}_{1/3}\text{Ni}_{1/3}\text{Mn}_{1/3}\text{O}_{2+\delta}$  phase, not  $\text{Ni}_{1/3}\text{Mn}_{1/3}\text{O}_{2+\delta}$  phase observed in undoped cathode. Figure 5 shows the Co, Ni, and Mn K-edge XANES spectra of the  $\text{Li}_x[\text{Ni}_{0.33}\text{Co}_{0.33}\text{Mn}_{0.30}\text{Mg}_{0.04}\text{O}]_{1.96}\text{F}_{0.04}$ , and the peak shape of B supports the formation of a less developed  $\text{Co}_3\text{O}_4$  phase than the  $\text{Li}_x[\text{Ni}_{1/3}\text{Co}_{1/3}\text{Mn}_{1/3}\text{O}]_2$  phase. However, the pre-edge peak position (A) and peak shape (B and C) of the Ni and Mn K-edge XANES spectra of the  $\text{Li}_x[\text{Ni}_{0.33}\text{Co}_{0.33}\text{Mn}_{0.30}\text{Mg}_{0.04}\text{O}]_{1.96}\text{F}_{0.04}$  after thermal annealing were similar to those of  $\text{Li}_x[\text{Ni}_{1/3}\text{Co}_{1/3}\text{Mn}_{1/3}\text{O}]_2$ , indicating that the oxidation states of Ni and Mn were  $\text{Ni}^{2+}$  and  $\text{Mn}^{4+}$ , respectively. The changes in the C peaks for the Ni, Co, and Mn K-edge XANES spectra of the both cathodes can be explained by a possible rearrangement of the Ni, Co, and Mn local structure.

Figure 6 shows the Fourier transform (FT) magnitude variations of the Co, Ni, and Mn K-edge  $k^3$ -weighted extended X-ray absorption fine structure (EXAFS) spectra between  $\text{Li}_x[\text{Ni}_{1/3}\text{Co}_{1/3}\text{Mn}_{1/3}\text{O}]_2$  (denoted as solid line) and Mg-/F-doped  $\text{Li}_x[\text{Ni}_{0.33}\text{Co}_{0.33}\text{Mn}_{0.30}\text{Mg}_{0.04}\text{O}]_{1.96}\text{F}_{0.04}$  (filled circle) for various thermal annealing temperatures. In the cathode systems, it was determined that the local structural variation around Co was effective for the thermal structural evolution among three transition metal ions, as shown in Fig. 6. For the pristine and fully delithiated  $\text{Li}_x[\text{Ni}_{1/3}\text{Co}_{1/3}\text{Mn}_{1/3}\text{O}]_2$ , FT magnitudes of Co K-edge  $k^3$ -weighted EXAFS spectra at  $\sim 1.5$  and  $\sim 2.5$  Å correspond to six coordinated oxygen of the nearest neighboring atoms around the Co atom, and edge-shared  $\text{CO}_6$  octahedra, respectively. On heating, the edge-shared FT peak intensity gradually decreases, while a new FT peak at  $\sim 3.2$  Å was generated with increasing heating temperature, corresponding to corner-shared  $\text{CoO}_6$  octahedra. The peak feature variations were closely related to decrease in the number of edge-

shared  $\text{CoO}_6$  octahedra and the atomic mixing between Li and Co sites by thermal heating. This fact indicates that the Co ions in the octahedral site of the  $\text{Ni}_{1/3}\text{Co}_{1/3}\text{Mn}_{1/3}\text{O}_2$  layer migrate into the Li vacant site upon thermal heating. This atomic migration leads to the coexistence of both edge-shared and corner-shared octahedral sites with the lattice which then results in the phase transition to a spinel  $\text{Co}_3\text{O}_4$  phase through atomic rearrangement at the respective annealing temperature. On the other hand, the FT peak features of the Ni and Mn K-edge  $k^3$ -weighted EXAFS spectra are basically similar with each other after the heating, which means both Ni and Mn ions remain in the layered octahedral site. As a result, thermal behavior of fully delithiated undoped  $[\text{Ni}_{1/3}\text{Co}_{1/3}\text{Mn}_{1/3}\text{O}]_2$  leads to cleavage of delocalized distribution of Co, Ni, and Mn ions in the octahedral layer and then Co atomic selective migration into Li vacant site, followed by phase separation to spinel  $\text{Co}_3\text{O}_4$  and O3-type  $\text{Ni}_{1/3}\text{Mn}_{1/3}\text{O}_{2+\delta}$  layered phases. This result is consistent with that the XRD patterns in Fig. 1.

On the other hand, Co, Mn and Ni K-edge  $k^3$ -weighted EXAFS

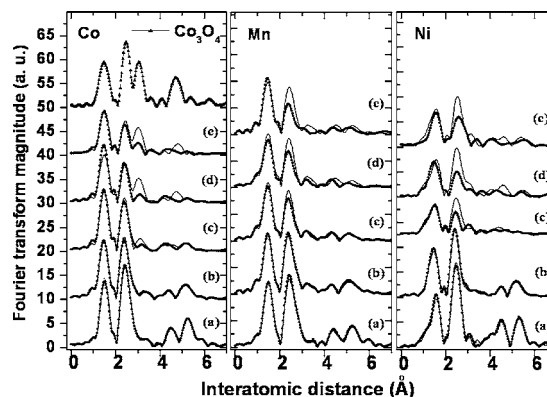


**Figure 6.** Fourier transform magnitudes of Co, Mn, and Ni K-edge EXAFS spectra for  $\text{Li}[\text{Ni}_{1/3}\text{Co}_{1/3}\text{Mn}_{1/3}\text{O}]_2$  (solid line) and  $\text{Li}_x[\text{Ni}_{0.33}\text{Co}_{0.33}\text{Mn}_{0.30}\text{Mg}_{0.04}\text{O}]_{1.96}\text{F}_{0.04}$  (filled circle): (a) before charging, (b) charging to 5 V, and (c) 200, (d) 300, and (e) 400°C heated samples.

spectra of the Mg-/F-doped  $\text{Li}_x[\text{Ni}_{0.33}\text{Co}_{0.33}\text{Mn}_{0.30}\text{Mg}_{0.04}]\text{O}_{1.96}\text{F}_{0.04}$  show basically similar FT peak features before and after heating. In particular, there is no FT peak development of corner-shared octahedral site in the Co K-edge. This means that the degree of phase transition into the spinel  $\text{Co}_3\text{O}_4$  phase by thermal heating relatively decreases in the Mg- and F-doped  $\text{Li}_x[\text{Ni}_{0.33}\text{Co}_{0.33}\text{Mn}_{0.30}\text{Mg}_{0.04}]\text{O}_{1.96}\text{F}_{0.04}$  with respect to the undoped  $\text{Li}_x[\text{Ni}_{1/3}\text{Co}_{1/3}\text{Mn}_{1/3}]\text{O}_2$ . After heating, FT peak features for Co, Ni, and Mn K-edge show overall layered  $\text{Ni}_{1/3}\text{Co}_{1/3}\text{Mn}_{1/3}\text{O}_2$  phase although the edge-shared FT peak intensities slightly decreases. This indicates that the Mg- and F-ions doping into the lattice prevents the migration of Co atom as well as Ni and Mn atoms into the Li vacant sites. As a result, the doped cathode can maintain the overall layered  $\text{Co}_{1/3}\text{Ni}_{1/3}\text{Mn}_{1/3}\text{O}_{2+\delta}$  phase even after thermal annealing.

### Conclusions

In fully delithiated conditions ( $x = 0$ ), upon thermal heating above  $200^\circ\text{C}$ ,  $\text{Li}_x[\text{Ni}_{1/3}\text{Co}_{1/3}\text{Mn}_{0.29}\text{Mg}_{0.04}]\text{O}_{1.96}\text{F}_{0.04}$  had better structural stability than  $\text{Li}_x[\text{Ni}_{1/3}\text{Co}_{1/3}\text{Mn}_{1/3}]\text{O}_2$ . Mg- and F-ions doping into the lattice prevented migration of Co atom, including Ni and Mn atoms into the Li vacant sites, leading to the maintenance of overall  $\text{Co}_{1/3}\text{Ni}_{1/3}\text{Mn}_{1/3}\text{O}_{2+\delta}$  phase layered phase. On the other hand,  $[\text{Ni}_{1/3}\text{Co}_{1/3}\text{Mn}_{1/3}]\text{O}_2$  showed cleavage of delocalized distribution of Co, Ni, and Mn ions in the octahedral layer and then Co atomic selective migration into Li vacant site, leading to spinel-like  $\text{Co}_3\text{O}_4$  phase formation. In consequence, Mg and F ions in the lattice led to the robust structural integrity even above  $200^\circ\text{C}$  in contrast to the undoped cathode that showed the phase decomposition into the spinel phase.

### Acknowledgment

The authors acknowledge the authorities at the Pohang Light Source (PLS) for the XAS measurements. This work was supported by University IT Research Center Project.

Kumoh National Institute of Technology assisted in meeting the publication costs of this article.

### References

1. Z. Zhang, Z. Gong, and Y. Yang, *J. Phys. Chem. B*, **108**, 17546 (2004).
2. Z. Zhang, H. S. Liu, Z. L. Gong, and Y. Yang, *J. Electrochem. Soc.*, **151**, A599 (2004).
3. J. Cho, Y.-W. Kim, B. Kim, J.-G. Lee, and B. Park, *Angew. Chem., Int. Ed.*, **42**, 1618 (2003).
4. J. Cho, H. Kim, and B. Park, *J. Electrochem. Soc.*, **151**, A1707 (2004).
5. J. Cho, T.-J. Kim, J. Kim, M. Noh, and B. Park, *J. Electrochem. Soc.*, **151**, A1899 (2004).
6. J.-G. Lee, B. Kim, J. Cho, Y.-W. Kim, and B. Park, *J. Electrochem. Soc.*, **151**, A801 (2004).
7. N. Takami, H. Inagaki, R. Ueno, and M. Kanda, Paper presented at the IMLB11-11th International Meeting on Lithium Batteries, Monterey, CA, June 23–28, 2002.
8. J. Cho, *Electrochem. Commun.*, **5**, 146 (2003).
9. J. Cho, *Electrochim. Acta*, **48**, 2807 (2003).
10. Z. Wang, Y. Sun, L. Chen, and X. Huang, *J. Electrochem. Soc.*, **151**, A914, 2004.
11. K. M. Shaju, G. V. Subba Rao, and B. V. R. Chowdari, *J. Electrochem. Soc.*, **151**, A1324 (2004).
12. K. M. Shaju, G. V. Subba Rao, and B. V. R. Chowdari, *Electrochim. Acta*, **48**, 145 (2002).
13. S. H. Park, C. S. Yoon, S. G. Kang, H.-S. Kim, S.-I. Moon, and Y.-K. Sun, *Electrochim. Acta*, **49**, 557 (2004).
14. J. Choi and A. Manthiram, *Electrochem. Solid-State Lett.*, **8**, C102 (2005).
15. N. Yabuuchi and T. Ohzuku, *J. Power Sources*, **119**, 171 (2003).
16. H. Maleki, G. Deng, A. Anani, and J. Howard, *J. Electrochem. Soc.*, **146**, 3224 (1999).
17. K.-K. Lee, W.-S. Yoon, and K.-B. Kim, *J. Electrochem. Soc.*, **148**, A1164 (2001).
18. G.-H. Kim, S. T. Myung, H. J. Bang, J. Prakash, and Y.-K. Sun, *Electrochem. Solid-State Lett.*, **7**, A477 (2004).
19. M. G. Kim, H. J. Shin, J.-H. Kim, S.-H. Park, and Y.-K. Sun, *J. Electrochem. Soc.*, **152**, A1320 (2005).
20. I. Belharouak, W. Lu, D. Vissers, and K. Amine, *Electrochem. Commun.*, **8**, 329 (2006).
21. G. G. Amatucci, J. M. Tarascon, and L. C. Klein, *J. Electrochem. Soc.*, **143**, 1114 (1996).